Precambrian Research 343 (2020) 105705

Contents lists available at ScienceDirect

Precambrian Research

journal homepage: www.elsevier.com/locate/precamres

# Hydrothermal circulation and oil migration at the root of the heterogeneous micro-structure of carbonaceous material in the 2.0 Ga Zaonega Formation, Onega Basin, Russia

Yuangao Qu[a,b,c], Mark A. van Zuilen[d,*], Aivo Lepland[e,f]

[a] Institute of Deep-sea Science and Engineering, Chinese Academy of Sciences, Sanya, China
[b] Department of Paleobiology, Swedish Museum of Natural History, Stockholm, Sweden
[c] Centre for Geobiology, Department of Earth Sciences, University of Bergen, Bergen, Norway
[d] Equipe Géomicrobiologie, Université de Paris, Institut de Physique du Globe de Paris, CNRS, Paris, France
[e] Geological Survey of Norway, Trondheim, Norway
[f] Department of Geology, University of Tartu, Tartu, Estonia

ARTICLE INFO

*Keywords:*
Proterozoic
Hydrothermal fluids
Carbonaceous material
Raman spectroscopy

ABSTRACT

Organic-rich rocks of the 2.0 Ga Zaonega Formation, Karelia, Russia, have been studied extensively to gain understanding of the global carbon cycle and reconstruction of paleo-environments, directly after the Great Oxidation Event (GOE). This formation has a complex history of alteration, involving pervasive hydrothermal circulation, hydrocarbon generation/migration, and mineral authigenesis. Several previous studies have focused on the description of these secondary effects, and the identification of primary geochemical signals in the carbonaceous phases. Migration and infiltration of organic-rich fluids appear to have had only limited effect on the primary carbon isotope record ($\delta^{13}C_{org}$). However, the structural variability of carbonaceous material (CM) appears to have been strongly affected, with a range of reported structures including carbon onion-shaped nanostructures and mineral-templated graphite films. Here we present a systematic Raman spectroscopy-based study of the structural variability of CM in a drill core representing the middle and upper strata of the Zaonega Formation. The Raman spectra of CM show a systematic difference in structural order between the bulk carbonaceous matrix (Matrix-CM) and the CM occurring near mineral contacts (Contact-CM), indicating that mineral templating was an important process affecting structural order in the formation. The templating effect was observed on the surface of a wide range of minerals. The difference in structural order between Matrix-CM and Contact-CM can be traced throughout the ca. 400 m stratigraphy. The structural order varied with the degree of alteration and hydrothermal circulation, from highly ordered structures directly above a large gabbro intrusion at the bottom of the stratigraphy to less ordered structures higher up in the sequence. This trend directly correlates with the $\delta^{18}O$ trend of secondary calcite, and can be attributed to the decreasing influence and temperature regime of hydrothermal circulation upward in the stratigraphy. The results presented here suggest that organic-rich hydrothermal fluids can locally strongly enhance graphitization of carbonaceous materials, and cause sample-scale heterogeneities in the structural order of organic materials. This has implications for the interpretation of carbonaceous materials in other ancient rocks experiencing circulation of organic-rich hydrothermal fluids.

## 1. Introduction

Organic-rich rocks of the 2.0 Ga Zaonega Formation, Karelia, Russia (Figs. 1 and 2), have been studied extensively to gain understanding of the global carbon cycle and reconstruction of paleo-environments, directly after the Great Oxidation Event (GOE). Carbon isotopes of carbonaceous material (CM) in the upper part of the formation record a major negative carbon isotope excursion ($\delta^{13}C_{org}$ from ca. –25 to –40‰, VPDB), which is variably explained by changes in the global carbon cycle (Kump et al., 2011) or local basinal increase in methanotrophy (Qu et al., 2012, 2018).

The Zaonega Formation has a complex history of alteration, involving syndepositional gabbro intrusions that caused pervasive hydrothermal circulation, hydrocarbon generation/migration and extensive

* Corresponding author.
*E-mail address:* vanzuilen@ipgp.fr (M.A. van Zuilen).

https://doi.org/10.1016/j.precamres.2020.105705
Received 26 February 2020; Accepted 17 March 2020
Available online 21 March 2020
0301-9268/ © 2020 The Authors. Published by Elsevier B.V. This is an open access article under the CC BY license (http://creativecommons.org/licenses/BY/4.0/).

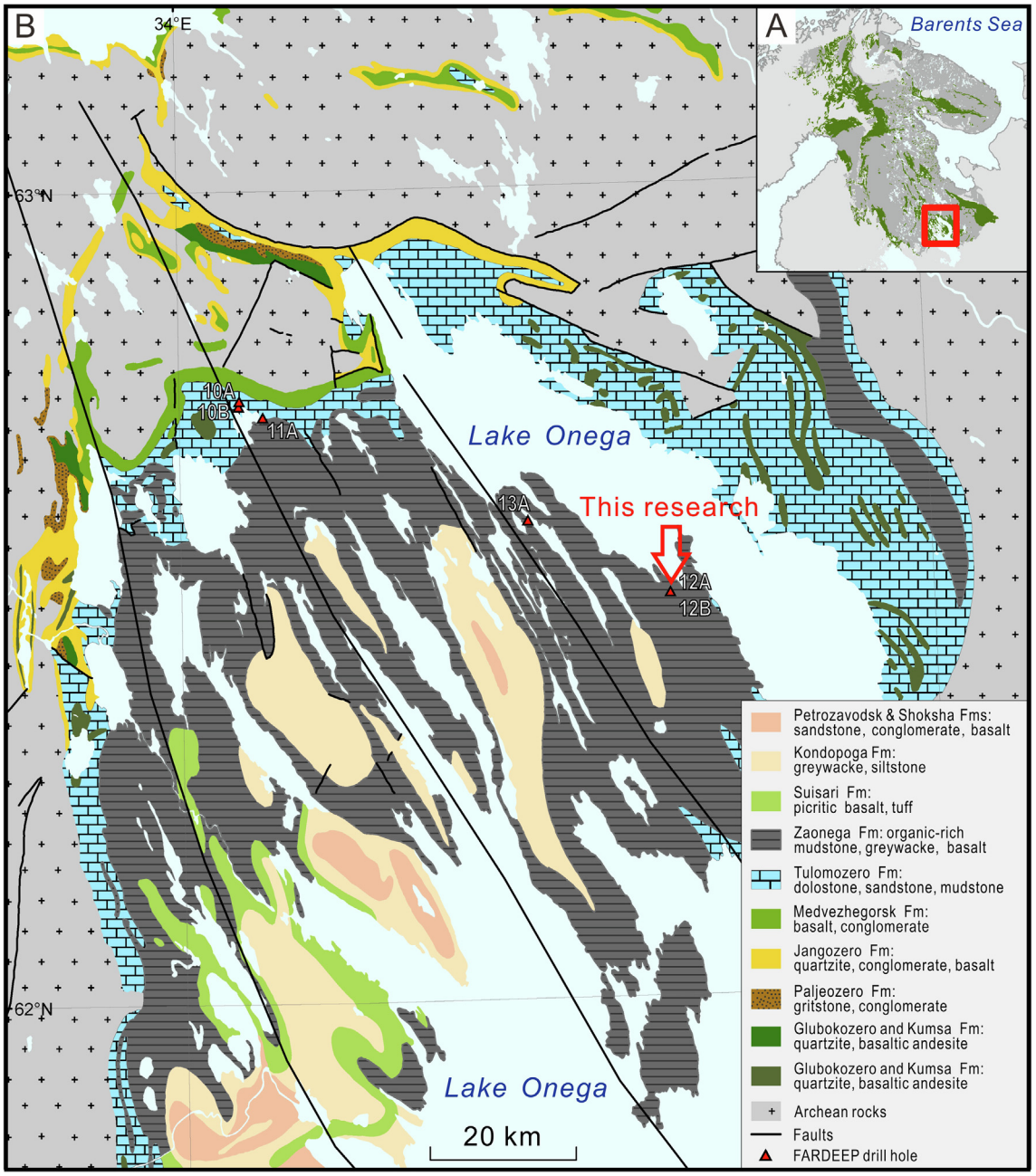


**Fig. 1.** Simplified geological map of the Onega Basin with the location of FAR-DEEP drill holes 12AB (red arrow). 'Fm' = 'Formation' (modified from Koistinen et al., 2001; Qu et al., 2012, 2018). (A) Regional inset map of the studied area. (B) Zoom in of the red box in (A). (For interpretation of the references to colour in this figure legend, the reader is referred to the web version of this article.)

mineral recrystallization and authigenesis in the adjacent organic-rich sediments. The formation has also experienced regional greenschist-facies metamorphism (Melezhik et al., 1999, 2012). Several studies have therefore focused on the description of these secondary effects, and the identification of primary signals in the carbonaceous phases. Studying micro-drilled samples throughout the Zaonega Formation, Qu et al. (2012) showed that the isotopic difference between the organic-rich veins and their host rocks appeared to be rather small (up to 1.1‰, typically < 0.5‰), indicating the remobilized CM in the veins largely originated from the directly surrounding sediments. A subsequent study using secondary ion mass spectrometry (SIMS), further confirmed that individual bulk samples showed limited isotopic heterogeneity (Qu et al., 2018). Migration and infiltration of organic-rich fluids therefore appear to have had only limited effect on the primary stratigraphic $\delta^{13}C_{org}$ trend.

The complex post-depositional history of the Zaonega Formation does, however, appear to have had a very significant effect on the structural variability of the carbonaceous phases. The CM-rich rocks in the formation, commonly known as 'shungite' (Buseck et al., 1997; Filippov and Golubev, 1994; Kovalevski et al., 2001), display various unusual structural characteristics, including non-graphitizing behavior (Khavari-Khorasani, 1979; Melezhik et al., 1999, 2004), carbon onion-shaped nanostructures (Kovalevski, 1994; Kovalevski et al., 2001), and the presence of mineral-templated graphite films (van Zuilen et al., 2012). It has been shown by Chazhengina and Kovalevski (2013) that contact metamorphism affected the structure of CM directly above gabbro intrusions within the formation. However, that study particularly focused on the bulk carbonaceous phase, and did not provide information on the sample scale heterogeneity in carbon structure, particularly near hydrothermally-formed mineral surfaces that have been

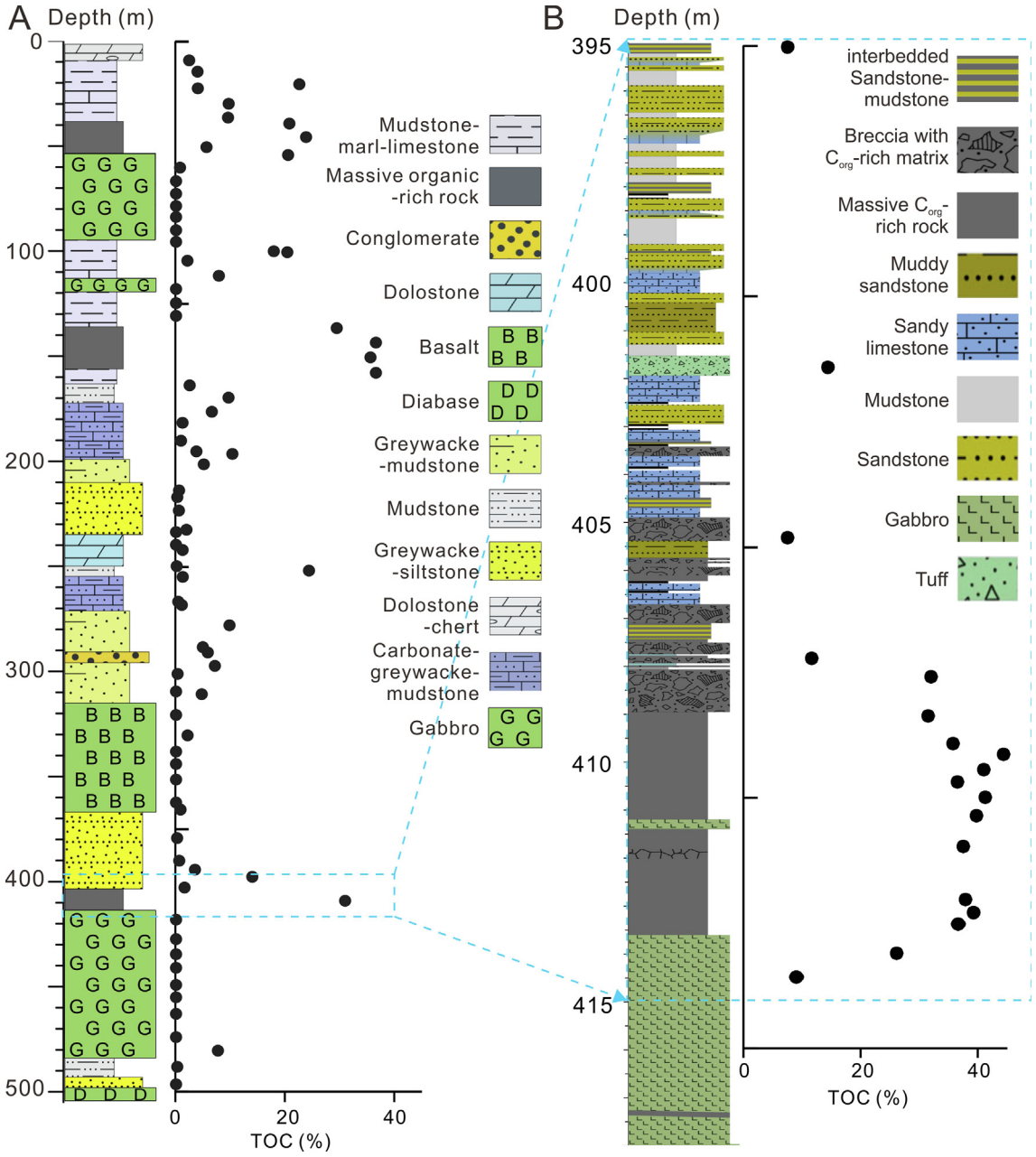


**Fig. 2.** Lithostratigraphy of the studied drill cores (stratigraphic columns revised after Qu et al., 2012, 2018). (A) Simplified lithostratigraphic column and total organic carbon (TOC) contents through the FAR-DEEP drill holes 12AB. (B) Detailed lithostratigraphic column of the organic-rich interval at 415–395 m depth.

shown to contain relatively highly ordered carbon films (van Zuilen et al., 2012). Also, hydrothermal circulation and oil migration operated on a larger basin-wide scale and thus affected the entire stratigraphy, not only the contacts near magmatic units.

Since it is known that mineral surfaces can initiate and accelerate localized graphitization of CM in rocks affected by hydrothermal circulation and hydrocarbon generation/migration (van Zuilen et al., 2012), it is therefore of interest to compare the structural variation of bulk CM fractions with carbon-mineral interfaces throughout the entire stratigraphy of the Zaonega Formation. This will shed light on the processes that formed a structurally highly unusual form of 'shungite' carbon, and in general will increase our understanding of graphitization processes in rocks experiencing hydrocarbon generation and hydrothermal alteration. This study has also general implications for the interpretation of Raman spectroscopy-based geothermometers and the characterization of organic remains in ancient hydrothermally affected petroleum system.

## 2. Background: the Raman spectrum of carbonized and graphitized materials

The process of carbonization of CM involves thermal cracking, loss of heteroatoms (H, N, O, P, and S), and aromatization, resulting in materials consisting of disordered aggregates of basic structural units (BSU, defined as units of 2–3 polyaromatic layers consisting of 4–10 rings each (Bustin et al., 1995)). At the onset of graphitization these BSUs will grow in size and start to align, until a defect-free triperiodic order is attained. This purely physical process of irreversible reorganization is referred to as 'graphitization' (Rouzaud et al., 2015). Temperature is the main driving force for carbonization and graphitization in metamorphic rocks (Beyssac et al., 2002; Wopenka and Pasteris, 1993). There are, however, other factors that can accelerate

carbonization and graphitization, such as strain (Bustin et al., 1995), hydrothermal fluid circulation (Olcott Marshall et al., 2014; Sforna et al., 2014), and mineral templating effects (van Zuilen et al., 2012). The effects that these processes have on carbonization and graphitization are less well known.

The Raman spectrum of CM has a distinct peak at 1580 $cm^{-1}$ representing in-plane $E_{2g}$ bond stretching of carbon in a graphite structure. It is therefore generally designated as the G-peak. Defects in the crystalline structure of graphite cause double resonance effects leading to the peaks at 1350 $cm^{-1}$ (D1) and 1620 $cm^{-1}$ (D2). In strongly disordered CM's with out-of-plane defects, tetrahedrally coordinated carbons, dangling bonds, and heteroatoms (e.g. H, O, N), a broad D3 peak at ~1500 $cm^{-1}$ and shoulders on the D1-peak can be observed (most notably a D4-peak at ~1250 $cm^{-1}$, but in highly disordered materials more peaks can be present) (Henry et al., 2019).

The spectral parameters of these combined D- and G-peaks and their intensity ratios have been used extensively to describe the structural characteristics and maturation state of CM in diagenetic and metamorphosed rocks (Baludikay et al., 2018; Beyssac et al., 2002; Delarue et al., 2016; Ferrari and Robertson, 2000; Foucher et al., 2015; Jehlička and Bény, 1992; Kouketsu et al., 2014; Lahfid et al., 2010; Qu et al., 2019; Sforna et al., 2014; Wopenka and Pasteris, 1993; Qu et al., 2015). In some studies a simple two-peak fit is employed (D-peak at 1350 $cm^{-1}$, G-peak at ca. 1600 $cm^{-1}$), linking the intensity ratio of the two peaks, ID/IG, to the average defect-bound crystal domain size of graphitic material (Ferrari and Robertson, 2000; Tuinstra and Koenig, 1970). Such an approach works well for materials that have experienced at least lower-greenschist-facies metamorphism. In most other studies a multi-peak deconvolution is performed, describing the G-peak and D1-peak, and the D2-, D3-, D4-, and D5-peaks depending on the maturation grade of the material. The degree of structural order of the CM can then be described by any parameter that quantifies the amount of defects (D-peaks) relative to the amount of pure graphite structure (G-peak), based on peak-intensity, -area, -full width at half maximum (FWHM), or -position. The FWHM of the G-peak itself is directly proportional to the degree of structural order of a graphitic material (Rouzaud et al., 2015). This indicator can only be measured, however, if precise deconvolution of the G-peak and the D2-peak has been made.

Since temperature is the main driver of carbonization and graphitization in metamorphosed rocks, several parameters have been proposed as a Raman-based geothermometer, such as FWHM-D1 (Kouketsu et al., 2014) or the peak area-based ratio R2 = D1/(G + D1 + D2) (Aoya et al., 2010; Beyssac et al., 2002). These parameters are good indicators to establish the degree of structural order of CM, but in strongly sheared or hydrothermally-altered rocks a direct inferred peak temperature should be interpreted with care.

In order to describe the structure of CM in the greenschist-facies Zaonega Formation, the following Raman spectral parameters were used: 1) a two-peak fit at 1350 $cm^{-1}$ and 1600 $cm^{-1}$ respectively and defining the intensity ratio I-1350/1600 in Fig. 3 (Foucher et al., 2015; Qu et al., 2015) that should be an indicator for graphite crystal domain size (Ferrari and Robertson, 2000); 2) decomposition of peaks in the spectral range between 1000 $cm^{-1}$ and 1800 $cm^{-1}$ into D4-, D1-, D3-, G- and D2-peaks and determination of FWHM-G (Fig. 3) (Rouzaud et al., 2015) and R2 from which tentative peak temperatures could be calculated using the relationship $T_{max}$ (°C) = -445*R2 + 641 (Fig. 3) (Beyssac et al., 2002).

The parallel graphene layers in a crystalline graphite structure can be artificially strongly affected by polishing when thin sections of rocks are prepared. In the uppermost layer of the graphite lattice (Ammar and Rouzaud, 2012; Maslova et al., 2012), a ca. 10 nm thick zone known as the 'Beilby' layer (Ammar and Rouzaud, 2012) is created, where the double resonance conditions of the lattice have been changed. Laser-light does not penetrate more than ca. 30 nm into an opaque material such as graphite (Colomban, 2002; Gouadec and Colomban, 2007). Light that falls on a polished graphite surface will thus generate a Raman spectrum from this Beilby layer with more intense double resonance-induced D-peaks. Only the G-peak remains unaffected, since it is directly dependent on sp2-bonding in the graphite structure (Ammar and Rouzaud, 2012). For less ordered CMs, where small graphite structural units are randomly ordered, this polishing-induced effect is much smaller or entirely absent. In order to effectively use Raman spectroscopy to characterize the CM of the Zaonega Formation, we therefore 1) carried out a polishing test to determine if D-peaks have been affected, and 2) use FWHM-G in addition to the other parameters to determine the degree of graphitic structural order.

## 3. Geological setting

The research area is located at the northern shore of the Lake Onega in central Karelia (Fig. 1), NW Russia, at the south-eastern margin of the Fennoscandian Shield. The Zaonega Formation is part of a supracrustal succession in the Paleoproterozoic Onega Basin, representing a rift-related basin on the margin of the Karelian craton, that was formed in the Paleoproterozoic during the opening of the Svecofennian Ocean (Melezhik et al., 1999). It has an overall thickness over 1500 m covering the area of 9000 $km^2$ (Melezhik et al., 1999; Koistinen et al., 2001).

The Zaonega Formation contains large accumulations of organic-rich sediments and records evidence of widespread petroleum generation, migration and accumulation (Melezhik et al., 2004; Qu et al., 2012). Widely distributed basalts, tuffs and gabbro intrusions with peperite contacts imply mafic magmatic activity coeval with sedimentation (Črne et al., 2013b, 2013a; Galdobina, 1987). Organic material in the sedimentary rocks experienced contact metamorphism and hydrocarbon generation induced by magmatic intrusions largely coeval with the sedimentation, and subsequent greenschist-facies metamorphism (Melezhik et al., 1999). Some intervals in the succession are highly organic-enriched (up to 75 wt% total organic carbon).

The organic-rich rocks of the Zaonega Formation provided a Re-Os age of ca. 2.05 Ga (Hannah et al., 2008). The Pb-Pb age from the underlying Tulomozero dolostones provides a maximum age of 2.09 ± 0.07 Ga (Ovchinnikova et al., 2007), whereas several Sm-Nd and Pb-Pb isochrons from the gabbro within the volcanic sequence of the overlying Suisari Formation constrain the minimum age at ca. 1.98 Ga (Puchtel et al., 1998, 1999). Considering that the Zaonega Formation postdates the Lomagundi-Jatuli $\delta^{13}C_{carb}$ excursion whose termination in Fennoscandia was dated to 2.06 Ga (Melezhik et al., 2007), the accumulation of the Zaonega sediments has been traditionally constrained to the 2.06–1.98 Ga time interval. Recent geochronology studies, however constrain the deposition of Zaonega sediments between 1.982 ± 0.0045 (tuff in the lower Zaonega Formation) and 1.967 ± 0.0035 Ga (detrital zircons in the Kondopoga Formation) (Martin et al., 2015).

## 4. Materials and methods

### 4.1. Materials

The studied materials were sampled from two overlapping drill cores 12A and 12B (62°29.711N, 31°17.460E, Figs. 1B and 2A), together representing a c. 500 m thick succession of the middle and upper strata of the Zaonega Formation (Fig. 2A). These cores (hereafter referred to as 12AB) were obtained during the "Fennoscandian Arctic Russia-Drilling Early Earth Project" (FAR-DEEP), a sub-project of the "International Continental Scientific Drilling Program" (ICDP). A total of 39 polished thin sections (200 μm thickness) were prepared for analyses by scanning electron microscopy (SEM) and Raman spectroscopy.

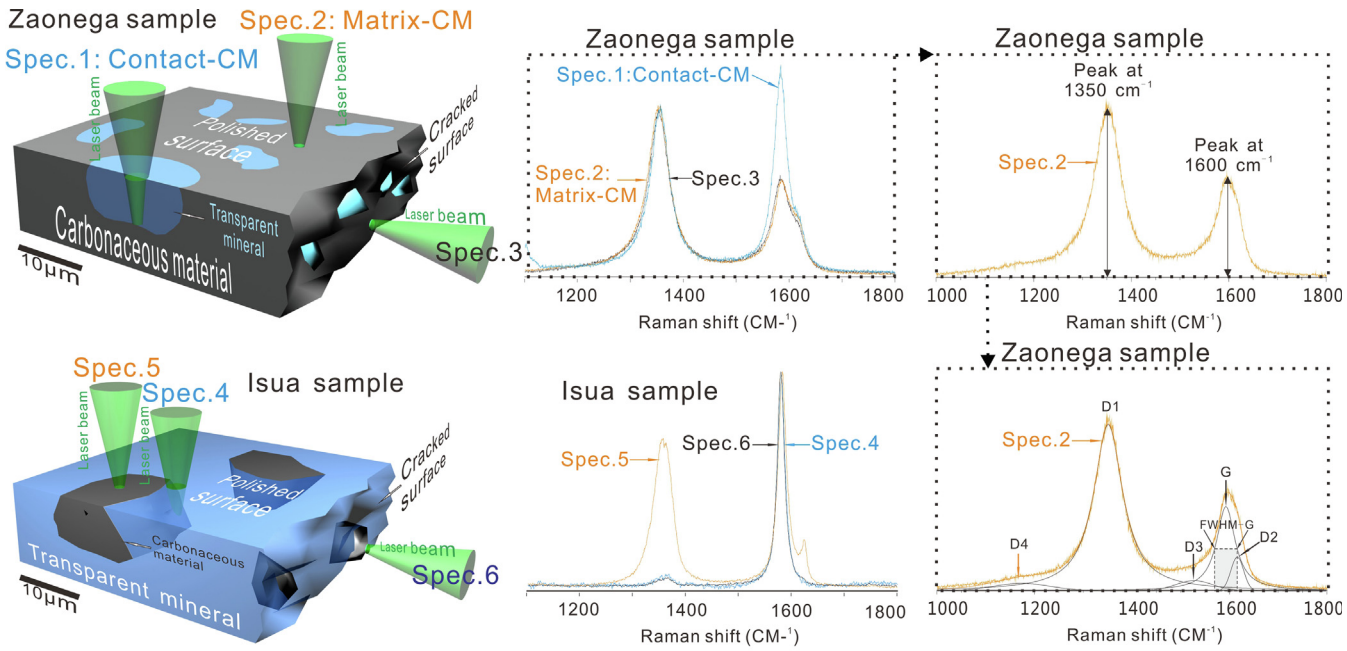


| | I-1350/1600 | R2 | FWHM-G | n | | I-1350/1600 | R2 | FWHM-G | n |
|---|---|---|---|---|---|---|---|---|---|
| Spec. 1 | 0.92±0.15 | 0.56±0.03 | 33.50±1.30 | 12 | Spec. 4 | 0.09±0.02 | 0.21±0.08 | 17.45±1.03 | 11 |
| Spec. 2 | 1.75±0.09 | 0.68±0.01 | 42.37±2.55 | 12 | Spec. 5 | 0.71±0.02 | 0.52±0.01 | 20.13±0.61 | 13 |
| Spec. 3 | 1.65±0.10 | 0.67±0.01 | 40.94±2.12 | 12 | Spec. 6 | 0.07±0.01 | 0.20±0.07 | 17.69±1.36 | 15 |

**Fig. 3.** Test of polishing and cracking artifacts on the structure of CM: A specific comparison is made here between a sample from the organic-rich part at 413 m depth of drill core 12AB of the Zaonega Formation, and a graphite-bearing metacarbonate from the 3.7 Ga Isua Supracrustal Belt, Western Greenland (amphibolite-facies metamorphism). Representative Raman spectra obtained at specific locations are: for the Zaonega Formation Spec. 1 Contact-CM at the subsurface, Spec. 2 Matrix-CM at the polished surface, Spec. 3 Matrix-CM at the freshly cracked surface; for the Isua Supracrustal Belt Spec. 4 Graphite at the subsurface, Spec. 5 Graphite at the polished surface, Spec. 6 Graphite at the freshly cracked surface. Listed below this are the average values of I-1350/1600, R2 and FWHM-G, standard deviations and measured numbers. In the dashed box, a representative Raman spectrum illustrates two different ways of deconvoluting the spectrum used in this study: 1) defining I-1350/1600 as the intensity ratio of peaks at 1350 $cm^{-1}$ and 1600 $cm^{-1}$; 2) decomposing the spectrum into D1-, D2-, D3-, D4- and G-peaks, and calculating the parameter R2 = D1/(G + D1 + D2) and FWHM-G = full width at half maximum of the G-peak.

### 4.2. Scanning Electron Microscopy

Backscattered electron imaging (BSE) was performed directly on polished thin sections using a Leo1450VP scanning electron microscope (SEM) at the Geological Survey of Norway, Trondheim, Norway, in low vacuum mode at 16 Pa, using an acceleration voltage of 15 kV, a beam current of 80 µA and a working distance of 8–13 mm.

### 4.3. Raman spectroscopy

Raman spectra were obtained on rock thin sections using a Horiba-Jobin Labram 800 HR Raman spectrometer and an Olympus BX41 petrographic microscope at the Centre for Geobiology, University of Bergen, Norway. Excitation was achieved with a 514 nm Ar-ion laser with the absolute laser power of 15–20 mW, through a density filter (D = 0.3), 100 × objective, reaching a final laser power of c. 2.5 mW (measured with a Coherent Lasercheck Analyser) in a ca. 1–2 µm spot on the sample. Spectral acquisition was performed in "multi-window" mode with 2 × 10 s running time and a spectral range of 100–2000 $cm^{-1}$, using an edge filter for 514 nm excitation wavelength at 100 $cm^{-1}$ cut-off, a 100 µm entrance slit, a 1800 lines/mm grating, and an air-cooled (–70 °C) 1024 × 256 pixel CCD array detector. For a comparative study on CM at mineral interfaces and CM in the bulk samples, the laser of the Raman spectrometer was focused 1) below the polished surface, through the transparent minerals on the CM-mineral contacts ('Contact-CM', Spec. 1 in Fig. 3), and 2) on the massive matrix CM at the polished surface ('Matrix-CM', Spec. 2 in Fig. 3). For possible artifacts in this analytical setup, see Section 4.4. The obtained spectral data were treated with the software "Lab Spec version 5.58.25". Spectra were baseline-subtracted by automatic polynomial fitting in order to remove the background fluorescence. Subsequent peak fitting and characterization was performed by peak-de-convolution using a Gaussian-Lorentzian function with 100 iterations per fit.

### 4.4. Test for polishing artifacts for Raman spectral analysis of CM

In order to assess possible sample preparation artifacts on the structure of CM in the samples studied here, a comparative test was made between one of the polished sections of the greenschist-facies Zaonega Formation (Zaonega CM) and a polished section containing well-ordered graphite from the amphibolite-facies 3.7 Ga Isua Supracrustal Belt, southern West Greenland (van Zuilen et al., 2005). For these two samples Raman spectral analysis was carried out at the polished surface, at a freshly cracked surface and at the mineral contact with the transparent phase in the subsurface, respectively (Fig. 3).

In the Isua graphite sample, the Raman spectra of the freshly cracked surface (Spec. 6 in Fig. 3) and the graphite-mineral contact at the subsurface (Spec. 4 in Fig. 3) are overlapping and have similar spectral parameters, demonstrating that cracking of the sample did not cause significant structural disordering. In contrast, the spectrum of graphite from the polished thin section surface (Spec. 5 in Fig. 3) has distinctly higher I-1350/1600 and R2, but similar FWHM-G values compared to the other two spectra, proving that polishing enhanced disorder in the graphite structure.

In the Zaonega CM sample, the Raman spectra of the cracked surface (Spec. 3 in Fig. 3) and the polished surface (Spec. 2 in Fig. 3) are similar, proving that polishing did not cause additional disorder. This is likely due to the fact that this Matrix-CM consists of already variably

oriented structural units. In contrast, the Raman spectrum of the subsurface Contact-CM at the mineral interface (Spec. 1 in Fig. 3) is very different. It has distinctly lower I-1350/1600, R2 and FWHM-G values, indicating a significantly higher structural order than the other two spectra. Given that the FWHM-G is normally unaffected by polishing, the lower FWHM-G of Contact-CM compared to Matrix- CM indicates a genuine feature related to a higher carbon structural order near the CM-mineral interface. These observations are in line with those of van Zuilen et al. (2012) where TEM images of Zaonega CM confirmed the presence of graphite films enveloping the mineral phases. These test results also demonstrate that representative structural information of Zaonega CM can be obtained using Raman spectra derived from the surface of polished thin sections.

## 5. Results

### 5.1. Petrography of CM

The studied drill core (FAR-DEEP 12AB) consists of a succession of siliciclastic and carbonate sedimentary rocks, predominantly greywacke and mudstone interbedded with dolostone and limestone. Sediment deposition occurred alongside with syndepositional mafic magmatism, and sedimentary units are interlayered with tuffs and lava flows and intersected by sills exhibiting peperite contacts with enclosing sediments (Fig. 2). Contact metamorphism near these magmatic bodies and associated hydrothermal circulation affected CM throughout the sequence, generating bitumen, oil and pyrolytic gas. Some of these fractions migrated through fractures, resulting in widespread pyrobitumen veins (Fig. 4A and B) and impregnated sediments forming massive organic-rich intervals in the stratigraphy (TOC up to 40%, Fig. 2). The largest gabbro sill occurs at 484–413 m (Fig. 2A), and its upper peperite contact indicates an intrusion into wet unconsolidated sediment. The circulation of hydrothermal fluids carrying hydrocarbons was most intense within this gabbro-sediment contact zone (413–407 m), and formed a particular focus for the current study (Fig. 2B). Above this, at 367–315 m (Fig. 2A), a lava flow occurs that had only limited thermal effect on the surrounding sediments. Higher up in the stratigraphy smaller intervals of gabbro sills (at 119–113 m and 95–54 m, respectively) occur (Fig. 2A). Emplacement of these latter intrusions are interpreted to have occurred relatively close to the sediment surface, and likely caused hydrothermal fluid circulation at relatively lower temperature and pressure regime compared to the largest gabbro at 484–413 mm.

In most of the sedimentary succession, the CM predominantly occurs as pyrobitumen filling the pore space (Fig. 4A and B) or as disseminated kerogen in the bedded sediments (Fig. 4C–E). However at the contact zones of gabbro sills (Fig. 2A and B), particularly at the top contacts where massive organic-rich rocks are found (Fig. 2B), the primary sedimentary structures have been completely obliterated during circulation of hydrothermal fluids carrying oil/bitumen (Fig. 4F). Contraction fractures (Fig. 4G) and fluid/gas cavities (Fig. 4H), which have been filled with CM and albite and/or calcite are common in such massive organic-rich rocks. The brecciated sedimentary clasts are abundant in the contact zone, some of which have preserved the remnant bedding from the primary sedimentary structures (Fig. 4E).

### 5.2. Micrometer-scale structural heterogeneities of CM

The Raman spectra of CM in the Zaonega Formation show a very clear, systematic difference in structural order between the Matrix-CM and Contact-CM. Contact-CM has lower D1- and D2-peaks relative to the G-peak, and the G-peak itself is narrower (Figs. 3 and 5). Two-dimensional Raman mapping has been performed in order to further investigate the distribution of CM (using 1600 $cm^{-1}$ peak intensity as a proxyas a proxy) and its micro-scale structural variation (intensity ratio of peak at 1350 $cm^{-1}$ vs. 1600 $cm^{-1}$, I-1350/1600) in relation to minerals such as quartz, albite, muscovite, titanite, amphibole, chlorite, calcite, tremolite, talc, and sphalerite (Table S2). Complete Raman spectra are shown for quartz, albite, muscovite and titanite in Fig. 5. There appears to be a clear shift to lower I-1350/1600 values (blue and green colors) near all of these minerals, as opposed to the adjacent Matrix-CM (yellow and red colors). The three Raman spectral indicators used here to quantify the structural order of CM: I-1350/1600, R2 and FWHM-G, all show this difference between Contact-CM and Matrix-CM, and reveal small differences in Contact-CM at the different types of mineral surfaces (Fig. 6G–I and Table S2). Minor mineral specific variability of Contact-CM structural order may indicate slightly different mineral templating effects depending on the mineral surfaces.

### 5.3. CM structure along the stratigraphy

Raman spectral analyses of the entire sample set show the variation in structure for both Contact-CM and Matrix-CM throughout the stratigraphy of the Zaonega Formation (Fig. 6A–F, Table S1). Contact-CM has an I-1350/1600 = 0.84–1.51, R2 = 0.53–0.68 and FWHM-G = 30.5–45.8. Slight variations are seen between different mineral types (Fig. 6G–I, Table S2); the Contact-CM on the surfaces of quartz and albite grains has slightly lower I-1350/1600, R2 and FWHM-G values than Contact-CM at the surfaces of chlorite and titanite (Fig. 6G–I, Table S2). The Matrix-CM has a I-1350/1600 = 1.57–1.93, R2 and FWHM-G in the range of 0.67–0.74, and 40.5–54.5 respectively (Fig. 6A–F, Table S1). There is thus a systematic difference observed throughout the stratigraphy, between Matrix-CM and Contact-CM for all three Raman-based parameters. These differences between the two types of CM are here defined as 'Dff-I-1350/1600' = I-1350/1600-Matrix-CM – I-1350/1600-Contact-CM, 'Dff-R2' = R2-Matrix-CM – R2-Contact-CM, and 'Dff-FWHM-G' = FWHM-G-Matrix-CM – FWHM-Contact-CM, respectively (Fig. 7).

In the interval directly above the gabbro contact at 413 m depth, the I-1350/1600, R2 and FWHM-G of both Contact-CM and Matrix-CM increase slightly from 413 to 407 m (Fig. 6D–F). The difference between the two types of CMs – represented by Dff-I-1350/1600, Dff-R2, and Dff-FWHM-G – is largest here (Fig. 7D–F) compared to the overlying stratigraphy. From 407 m to the top of the stratigraphy, the absolute values of I-1350/1600, R2 and FWHM-G of both Contact-CM and Matrix-CM (Fig. 6A–C) are variable, but the difference between the two types of CM's – represented by Dff-I-1350/1600, Dff-R2, and Dff-FWHM-G - shows a systematic decreasing trend upwards along the stratigraphy (Fig. 7A–C).

## 6. Discussion

### 6.1. Two types of structural CM in the Zaonega Formation

The Matrix-CM of the Zaonega Formation has average values for the parameters I-1350/1600, R2, and FWHM-G that are in line with greenschist-facies metamorphism (Fig. 6A–F). Using the range of the parameter R2 for all measured Matrix-CM and the geothermometer of Beyssac et al. (2002) a tentative peak metamorphic temperature $T_{max}$ = 311–343 °C was calculated (Fig. 6B). As was pointed out in section 2 (Background), hydrothermal circulation can enhance carbonization and graphitization, and therefore these temperature values could be overestimated. Nevertheless, the calculated temperature range fits well with other estimates of regional metamorphism (Melezhik et al., 1999).

In contrast, Contact-CM in the Zaonega Formation, has a systematically higher degree of structural order, that is observed in all three parameters I-1350/1600, R2, and FWHM-G (Fig. 6A–F). Using the same R2-based geothermometer (Beyssac et al., 2002), the Contact-CM yields a $T_{max}$ = 339–405 °C (Fig. 6B). This is significantly higher than the $T_{max}$ calculated from Matrix-CM throughout the entire stratigraphy. It is

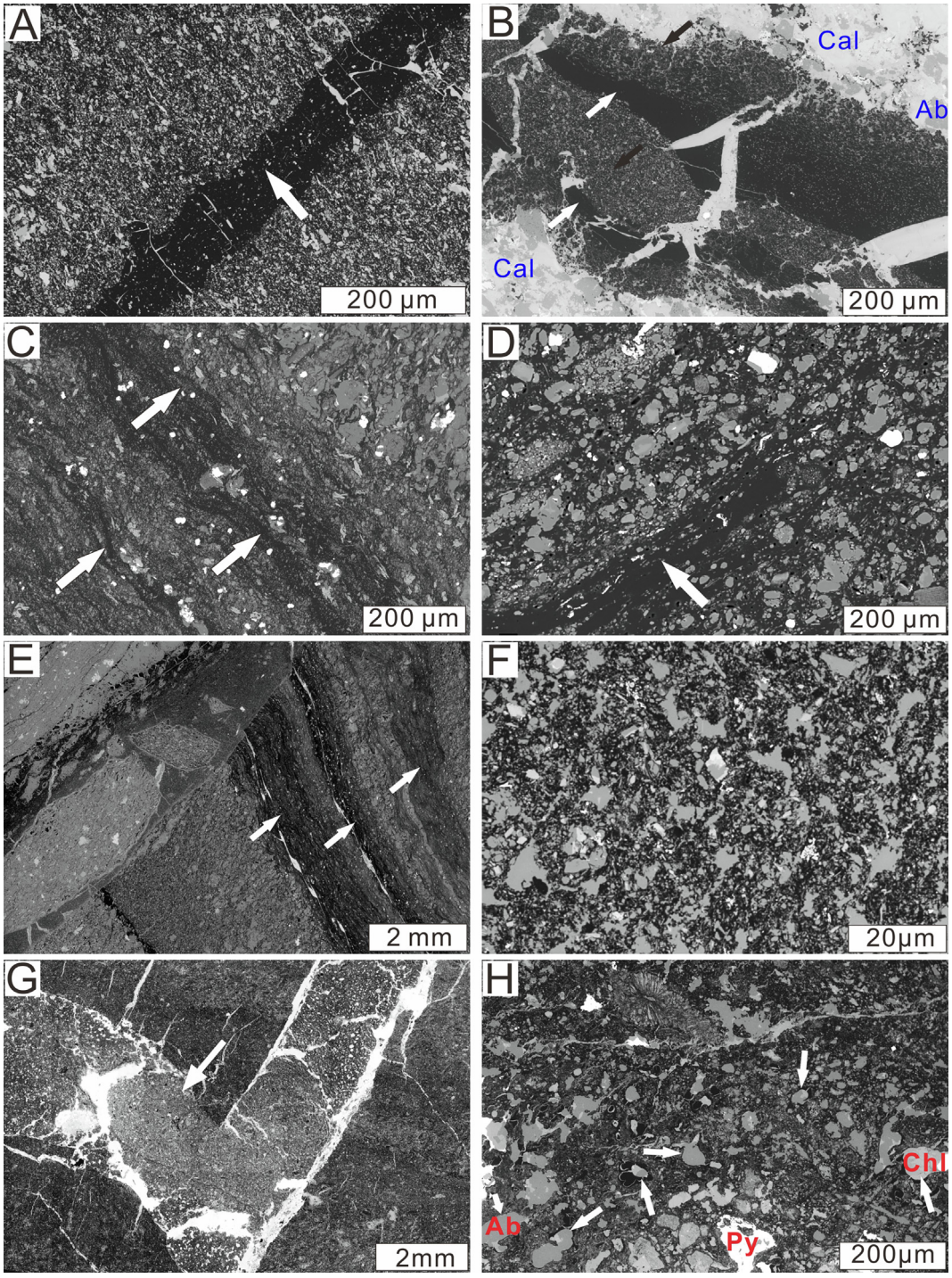


**Fig. 4.** Scanning electron microscopy images obtained in backscattered electron mode (SEM-BSE) showing petrographic associations of CM in the studied samples. (A) CM vein (arrow) at depth 410 m, cutting a massive organic-rich rock. (B) Calcite-albite dominated host rock at depth 400.13 m, containing a layered CM-rich vein, cut by a later generation of calcite-chlorite-quartz veins. The CM-rich vein varies from pure black CM (white arrow) to impure, silicate-rich grey CM (black arrow). (C) and (D) CM preserved in the sedimentary lamina (white arrows) at depth 408.38 m and 138.55 m respectively. (E) Brecciated clasts within massive, organic-rich matrix at depth 408.38 m. The clast on the right side of the image exhibits distinct laminations (white arrows) as CM-rich fine grained sandstone and siltstone laminae alternate. (F) Massive organic-rich rock at depth 413.11 m, consisting primarily of CM (black) and intergrown albite (grey). (G) Contraction fracture (arrow) within a massive organic-rich rock at depth 413.11 m, which was later filled with massive rock containing more silicates and less CM than the host rock. This was then rimmed by the latest generation albite-chlorite-tremolite-pyrite veins (bright). (H) Massive organic-rich rock depth 408.93 m, containing rounded fluid cavities (arrows), which are rimmed or filled either with CM, albite, chlorite or pyrite. Abbreviations Cal = calcite, Ab = albite, Chl = chlorite, Py = pyrite.

impossible that two such significantly different R2-based peak-temperatures are the result of one regional metamorphic event. It was shown before by van van Zuilen et al. (2012), using both Raman spectroscopy and TEM on samples from two different stratigraphic levels of the Zaonega Formation, that thin graphite films coat the surfaces of quartz and chlorite minerals. At a depth of 140 m in the core the graphite films were 15 ± 5 nm, and at a depth of 413 m, directly above a gabbro intrusion, the films were 25 ± 10 nm thick. In that

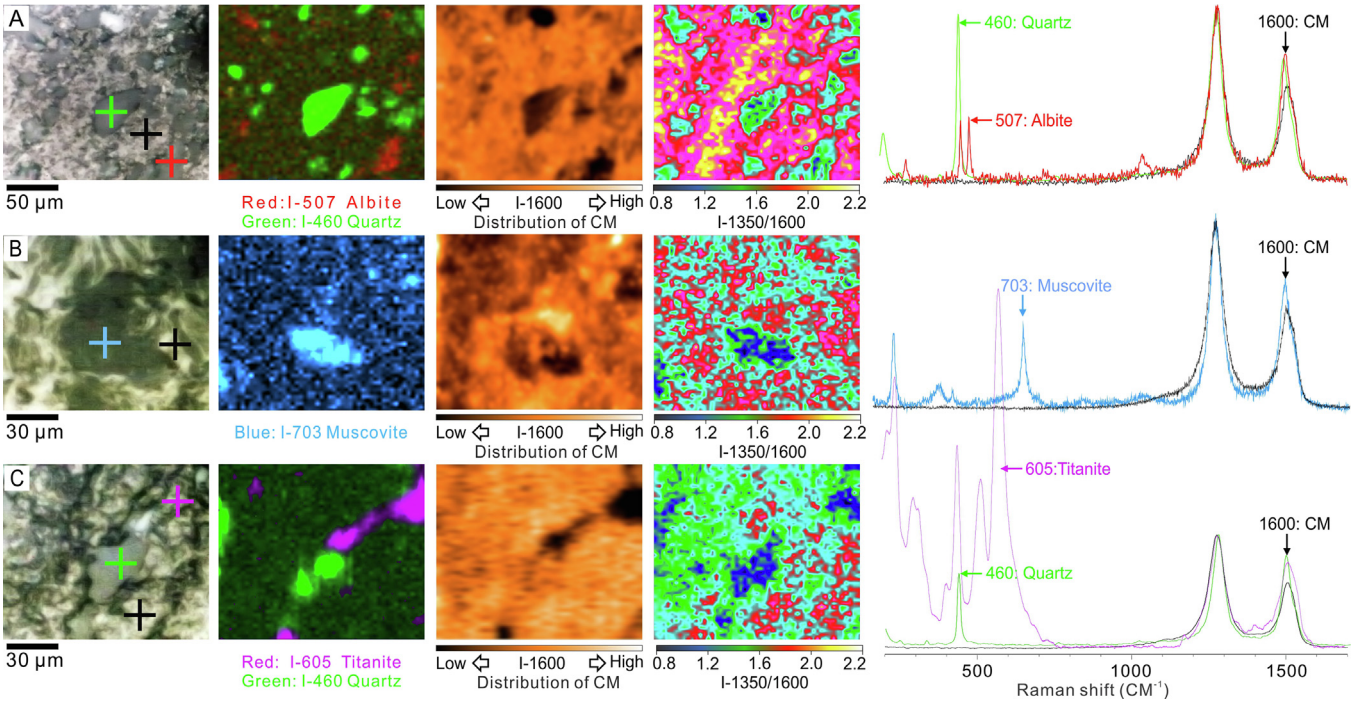


**Fig. 5.** Selected Raman spectra and Raman hyperspectral maps of Contact-CM and Matrix-CM in relation to various mineral phases within the massive organic-rich parts of the Zaonega Formation. Reflected light petrographic images (first column) show the locations of Raman spectral point analyses of Matrix-CM (black cross) and Contact-CM (colored crosses). These analyses were made as described in paragraph 4.4. The corresponding two-dimensional Raman hyperspectral maps show the distribution of mineral phases (second column), the distribution of CM (third column) as indicated by I-1600 (intensity at 1600 $cm^{-1}$), and its structural order (fourth column) described by I-1350/1600. (A) Sample at 103.8 m. The spatial distribution of CM relative to quartz (green, peak at 460 $cm^{-1}$) and albite (red, peak at 507 $cm^{-1}$). (B) Sample at 164.57 m. The spatial distribution of CM relative to muscovite (blue, peaks at 703 $cm^{-1}$). (C) Sample at 331.5 m. The spatial distribution of CM relative to quartz and titanite (purple, peak at 605 $cm^{-1}$). (For interpretation of the references to colour in this figure legend, the reader is referred to the web version of this article.)

study it was suggested that hydrocarbon-rich hydrothermal fluids likely facilitated the absorption and parallel alignment of precursor organic macro-molecules onto the charged surfaces of quartz and chlorite, leading to enhanced graphitization during contact metamorphism induced by gabbro intrusions and subsequent regional metamorphism (van Zuilen et al., 2012). Since laser light penetrates to ca. 30 nm into a graphite structure (Colomban, 2002; Gouadec and Colomban, 2007), and analyses on Contact-CM were made through the transparent mineral phase (Spec. 1 Fig. 3), likely some light penetrated through the films and scattered from the directly underlying Matrix-CM. It is therefore likely that Raman spectra of Contact-CM studied here represent a combination of pure graphite films and the underlying disordered Matrix-CM. The thicker the graphite film, the more ordered this combined Raman spectral signal becomes, resulting in lower I-1350/I-1580 intensity ratios, lower R2 values, and lower FWHM-G values. The variation in these parameters for Contact-CM throughout the stratigraphy, therefore reflect the variation in hydrothermally-induced mineral surface-templated graphitization.

### 6.2. Graphite films on different mineral surfaces

Detailed analysis of Contact-CM throughout the Zaonega Formation stratigraphy shows that graphite films were forming on all mineral surfaces, wherever bitumen was migrating and mixing with other fluids and mineral authigenesis was taking place. The Contact-CM on the surfaces of quartz and albite has a slightly higher structural order than that on the surfaces of chlorite and titanite (Fig. 6G–I, Table S2), suggesting that graphitization is more efficient on these first two mineral types. Either this reflects more defect-free crystalline graphite films, or the graphite films are thicker limiting the light penetration and hence the signal from the underlying Matrix-CM. Either way, these slight structural differences among Contact-CM are probably caused by mineral-specific differences in surface charge that influence binding and orienting of large organic molecules within the bituminous phase. Overall, organic-rich hydrothermal fluids appear to be the primary driving force for mineral-templated graphitization. The spectral differences between Contact-CM and Matrix-CM, defined as 'Dff' (see Methods, Fig. 7), can then be used to determine the extent of hydrothermal alteration that acted on the CM in addition to regional metamorphic alteration.

### 6.3. Variation in CM structure throughout the Zaonega Formation stratigraphy

It was already observed by van Zuilen et al. (2012) that Contact-CM in a sample occurring directly above the gabbro intrusion in the Zaonega Formation represented the thickest graphite films. The new data set presented here, now provides a more detailed picture of CM variation in contact zones, and enables to follow the effects of organic-rich hydrothermal fluid circulation throughout the stratigraphy. The massive organic-rich interval (407–413 m) above the gabbro, which has been pervasively altered by hydrothermal and bituminous fluids, has the largest observed difference between Contact-CM and Matrix-CM with the highest Dff-I-1350/1600, Dff-R2, Dff-FWHM-G values in the entire sequence (Fig. 7D–F). This suggests that the strongest hydrothermally-induced mineral-templating effect took place in this zone (Fig. 7D–F).

Stratigraphically upwards, above the massive altered zone (407–413 m), there is a systematic decrease in Dff-I-1350/1600, Dff-R2, Dff-FWHM-G across ca. 400 m of the rock section (Fig. 7A–C). The gabbro sill contact at 54 m, did not cause any contact specific structural changes in the CM in directly overlying sediments (Figs. 6 and 7). This

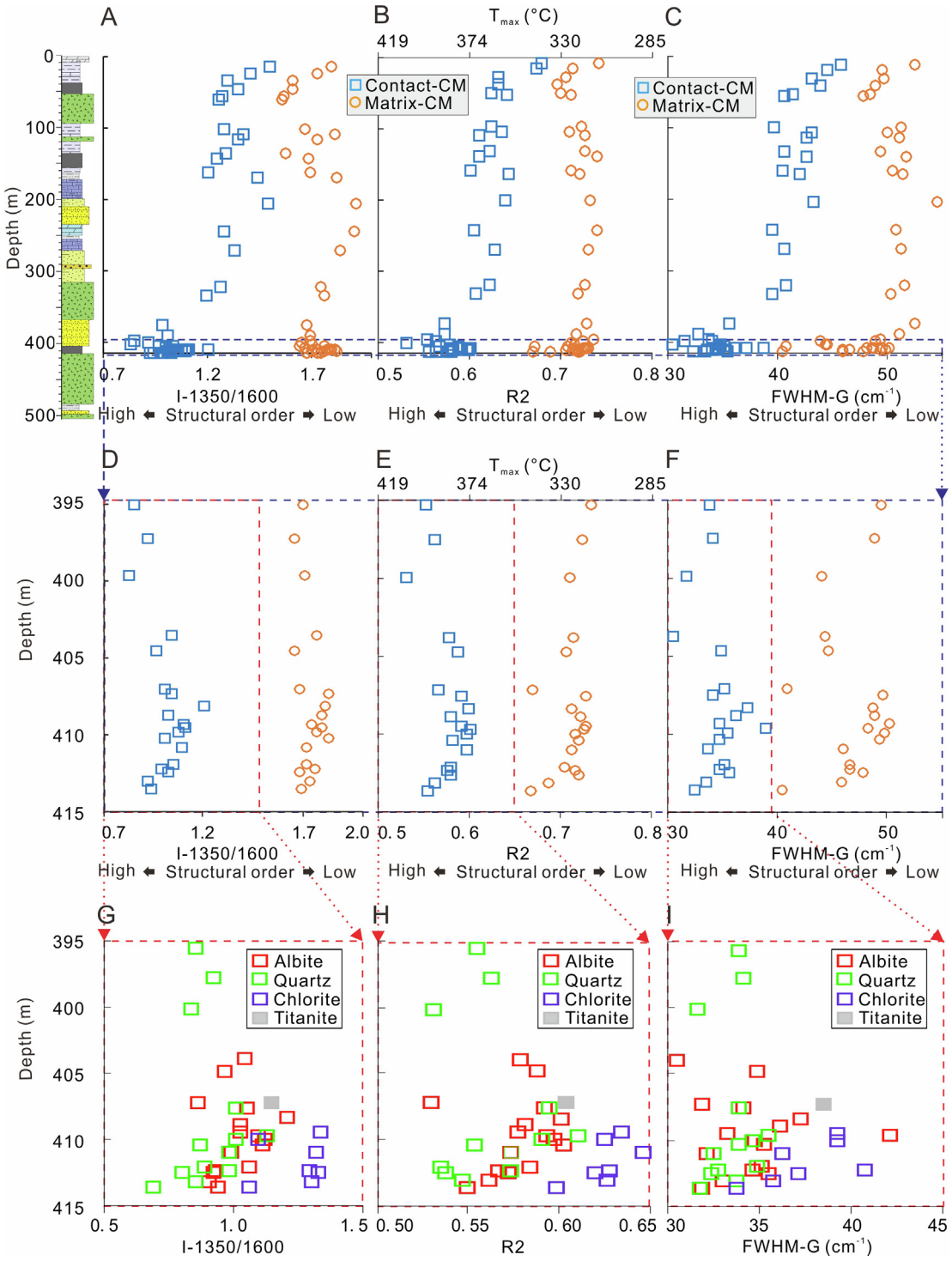


**Fig. 6.** Lithostratigraphy of the studied drill cores with average values of the key Raman parameters of CM as listed in Tables S1 and S2. (A)–(C) I-1350/1600, R2 and FWHM-G of CM along the core depth. (D)–(F) Zoom in of the interval (415–395 m depth) above the gabbro sill. (G)–(I) The average values of I-1350/1600, R2 and FWHM-G of Contact-CM at various mineral contacts.

suggests the process of mineral template-induced graphitization was less significant within this contact zone, likely because this sill intruded at shallower depth and lower temperature and pressure regime. CM in the sediments directly underlying the basaltic lava flow at 365 m also do not show any significant change in structure. Overall, it is thus concluded that enhanced mineral-templated graphitization was primarily driven by high-pressure hydrothermal fluids that were generated above the deeper gabbro contact at 413 m depth.

### 6.4. Contact metamorphism and hydrothermal circulation

The upward-decreasing trend in the structure of CM in the stratigraphy of the Zaonega Formation (Fig. 6A–C) coincides with a ca. 5‰ increase in $\delta^{18}O$ (Fig. 8A) of secondary calcite (Fallick et al., 2016). Although the initial interpretation of this $\delta^{18}O$ trend implied low temperature, post-metamorphic formation of secondary calcite (Fallick et al., 2016), the recent study by (Kreitsmann et al., 2019) links calcite formation in the upper part of the succession to hydrothermal

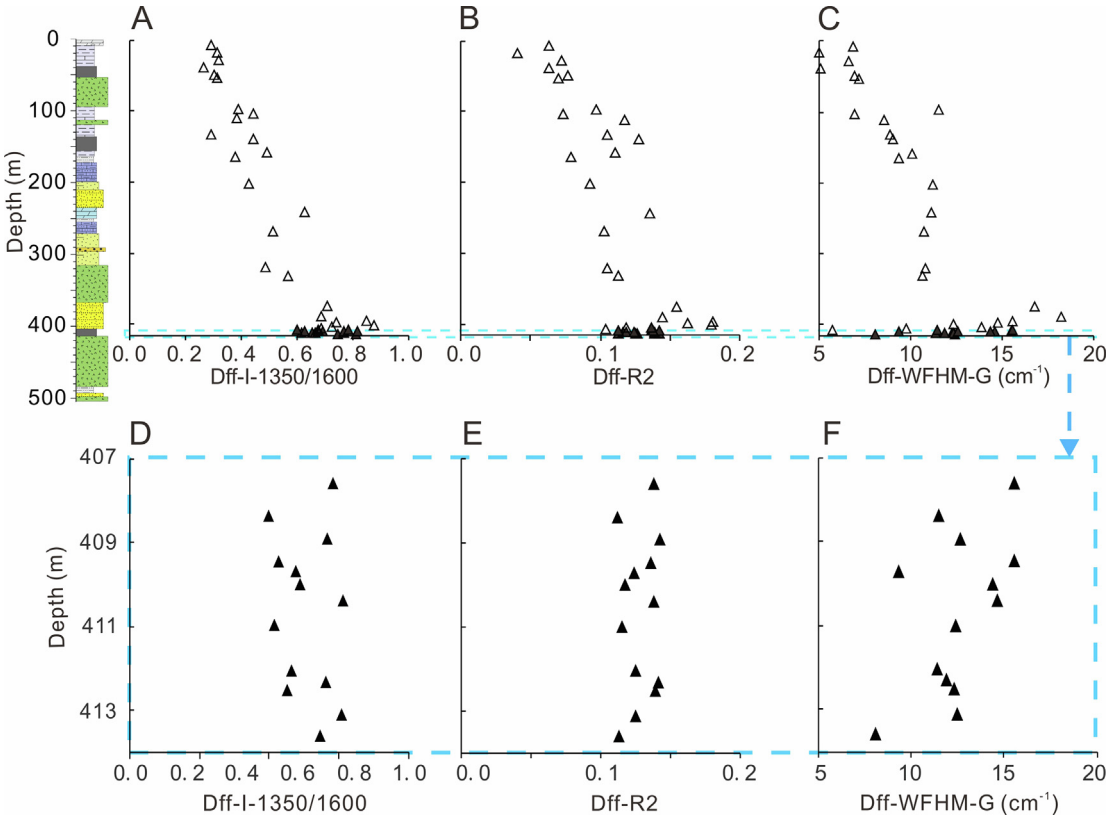


**Fig. 7.** The difference in structural order between Matrix-CM and Contact-CM in each sample as reflected by Dff-I-1350/1600 (I-1350/1600 of Matrix-CM – I-1350/1600 of Contact-CM), Dff-R2 (R2 of Matrix-CM – R2 of Contact-CM) and Dff-WFHM-G (WFHM-G of Matrix-CM – WFHM-G of Contact-CM).

circulation and dedolomitization under a 215–380 °C temperature regime. Calcite formation through hydrothermally triggered dedolomitization has been documented throughout the 12AB succession (Črne et al., 2014), and therefore it is likely the $\delta^{18}O$ trend reflects a systematic change in the isotopic composition of the hydrothermal fluids and/or upward decrease in the temperature of hydrothermal circulation. Hydrothermal circulation was likely triggered by the contemporaneous gabbro intrusion at depth, and therefore affected the deeper part of the sedimentary sequence more strongly than the upper part. Our results presented here, therefore show that Raman-based parameters of CM, particularly those of Contact-CM and the Dff values between Matrix-CM and Contact-CM, provide a direct indicator for hydrothermally-induced and mineral-templated graphitization throughout the stratigraphy of the Zaonega Formation.

The upward-decreasing trend in the structure of CM does not, however, correlate with the variation in $\delta^{13}C$ of CM throughout the core (Fig. 8B). It was already observed by Qu et al. (2012, 2018) that primary $\delta^{13}C$ values were not significantly altered, and rather reflect variations in the relative importance of methanotrophic and phototrophic microorganisms. Only near the contact with the lowermost gabbro sill at 413 m core depth there is a slight shift in $\delta^{13}C_{org}$ of 3‰ (Fig. 8B and F), that correlates well with the shift in absolute Raman spectral parameters (Figs. 6D–F and 8F–G) but not with the Raman spectral differences 'Dff' between Matrix-CM and Contact-CM (Figs. 7D–F and 8F).

This clearly indicates that contact metamorphism in the direct vicinity of the gabbro sill caused direct thermally-driven carbonization and graphitization of the bulk CM and thus affected both Matrix-CM and Contact-CM. This was accompanied by thermal cracking and the release of isotopically light $CH_4$, causing the observed shift towards higher $\delta^{13}C$ of the residual CM (Fig. 8F). Hydrothermal circulation higher above this contact apparently did not cause strong thermal cracking effects, but specifically caused graphitization at mineral interfaces. This explains why $\delta^{13}C$ values of CM in the remainder of the stratigraphy have not changed much, and still represent primary biomass. Our results presented here, therefore show that Raman-based parameters of CM – particularly the difference between Contact-CM and Matrix-CM – provide a direct indicator for contact metamorphism-induced carbonization and graphitization.

## 7. Conclusions

It is shown here using Raman spectroscopy-based parameters that variation in CM structural order varies systematically with intensity of hydrothermal circulation, from highly ordered structures in a massive organic-rich interval directly above a gabbro intrusion at the bottom of the stratigraphy to less ordered structures higher up in the sequence. This trend directly correlates with the $\delta^{18}O$ trend of secondary calcite, and can be attributed to the decreasing influence and temperature regime of hydrothermal circulation upward in the stratigraphy. The increased structural order is the result of hydrothermally-induced graphitization at the surfaces of authigenic minerals, as was suggested before (van Zuilen et al., 2012). The small variation among different mineral types, suggests that mineral surface charge affects the efficiency of parallel orientation of precursor organic molecules. The large trends in $\delta^{13}C_{org}$ throughout the stratigraphy of the Zaonega Formation, as reported earlier (Qu et al., 2012, 2018), apparently have not been strongly affected by this hydrothermal circulation. Only at the direct contact with the gabbro intrusion a small 3 ‰ shift in $\delta^{13}C_{org}$ was observed, but no systematic correlation with CM structure, nor the $\delta^{18}O$ of carbonates, was seen throughout the stratigraphy. This means that large $\delta^{13}C$ variations are indeed reflecting a shift in primary biomass, as was concluded earlier (Qu et al., 2012, 2018).

The results presented here suggest that hydrothermal organic-rich fluids can locally strongly enhance graphitization of carbonaceous materials. This is an important observation, that could possibly occur in

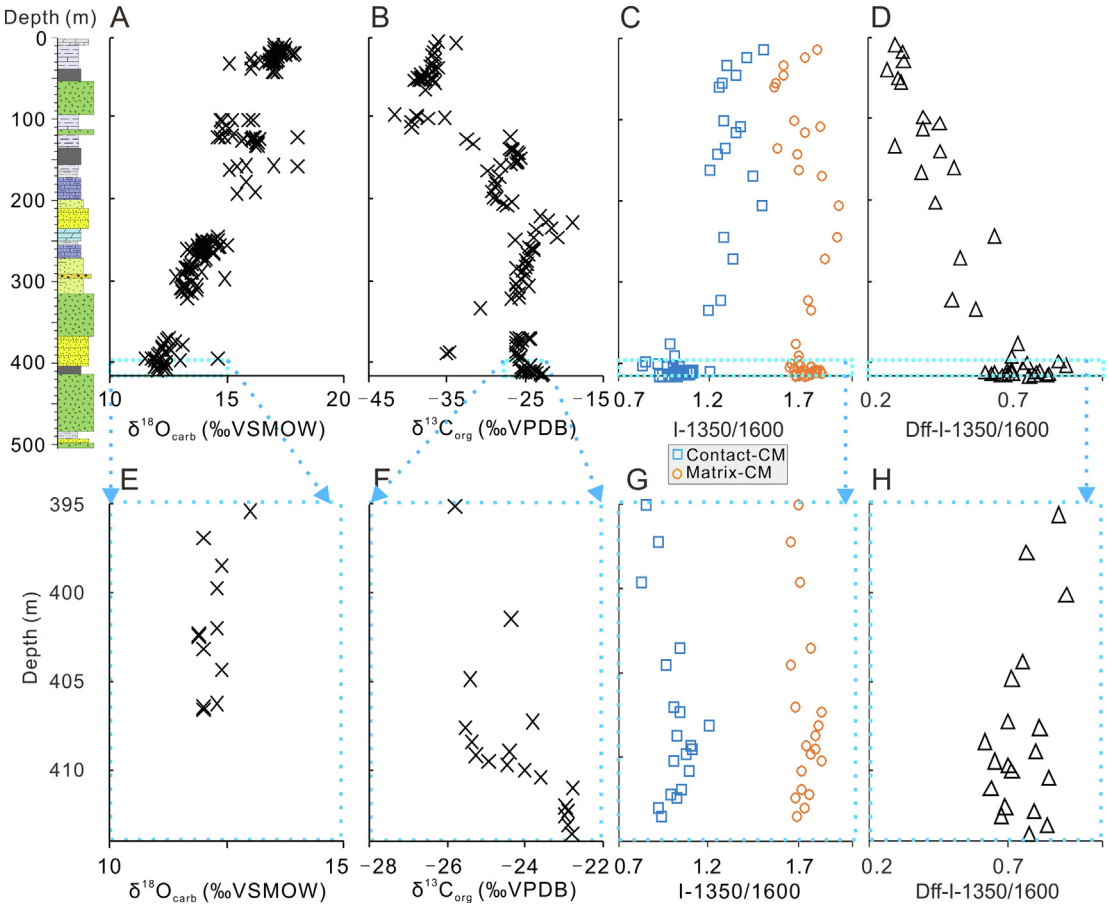


**Fig. 8.** Plots of carbonate $\delta^{18}O$ (A), $\delta^{13}C_{org}$ (B), I-1350/1600 (C) and Dff-I-1350/1600 (D) trends throughout the Zaonega Formation ($\delta^{18}O$ data from Fallick et al., 2016, $\delta^{13}C_{org}$ data from Qu et al., 2012). (E–H) Zoom in of the interval (415–395 m depth) above the gabbro sill.

other strongly hydrothermally-influenced rocks. CM occurs ubiquitously in chert deposits and chert-veins in Archean greenstone belts. Most of these rocks have been strongly affected by hydrothermal circulation (Brasier et al., 2005; Duda et al., 2018; Olcott Marshall et al., 2014; Sforna et al., 2014; Ueno et al., 2006; van den Boorn et al., 2007). Based on our results we predict that small variations in structural order could exist in the CM fractions in these types of rocks, as a result of hydrothermal alteration and localized bitumen migration. Another important implication is that hydrothermal fluid-induced graphitization apparently influences Raman-based geothermometers.

## Declaration of Competing Interest

The authors declare that they have no known competing financial interests or personal relationships that could have appeared to influence the work reported in this paper.

## Acknowledgment

This study was based on samples from the ICDP FAR-DEEP drilling project in Karelia, Russia. We thank members of the FAR-DEEP central science team and principal investigator V. Melezhik for coordinating this project and A. Crne for discussions about the geology of the Zaonega Formation. Y.Q is financially supported by the National Key R &D Program (2018YFC0309800), the National Natural Science Foundation of China (Grant No. 41972204), the Hundred Talent Program C (Y810011BRC) of China. We highly appreciate the technical help in the Geological Survey of Norway in Trondheim, the Centre for Geobiology in the University of Bergen and the Institute of Deep-Sea Science and Engineering, CAS. M.Z acknowledges support from the European Research Council under the European Union's Horizon 2020 Research and Innovation Program (grant agreement 646894).

## Appendix A. Supplementary data

Supplementary data to this article can be found online at https://doi.org/10.1016/j.precamres.2020.105705.

## References

Ammar, M.R., Rouzaud, J.N., 2012. How to obtain a reliable structural characterization of polished graphitized carbons by Raman microspectroscopy. J. Raman Spectrosc. 43, 207–211.

Aoya, M., Kouketsu, Y., Endo, S., Shimizu, H., Mizukami, T., Nakamura, D., Wallis, S., 2010. Extending the applicability of the Raman carbonaceous-material geothermometer using data from contact metamorphic rocks. J. Metamorph. Geol. 28, 895–914.

Baludikay, B., François, C., Sforna, M., Beghin, J., Cornet, Y., Storme, J., Fagel, N., Fontaine, F., Littke, R., Baudet, D., Delvaux, D., Javaux, E., 2018. Raman microspectroscopy, bitumen reflectance and illite crystallinity scale: comparison of different geothermometry methods on fossiliferous Proterozoic sedimentary basins (DR Congo, Mauretania and Australia). Int. J. Coal Geol. 191, 80–94.

Beyssac, O., Goffé, B., Chopin, C., Rouzaud, J.N., 2002. Raman spectra of carbonaceous material in metasediments: a new geothermometer. J. Metamorph. Geol. 20, 859–871.

Brasier, M.D., Green, O.R., Lindsay, J.F., McLoughlin, N., Steele, A., Stoakes, C., 2005. Critical testing of Earth's oldest putative fossil assemblage from the ~3.5 Ga Apex chert, Chinaman Creek Western Australia. Precambrian Res. 140, 55–102.

Buseck, P.R., Galdobina, L.P., Kovalevski, V.V., Rozhkova, N.N., Valley, J.W., Zaidenberg, A.Z., 1997. Shungites; the C-rich rocks of Karelia, Russia. Can. Mineral. 35, 1363–1378.

Bustin, R.M., Rouzaud, J.N., Ross, J.V., 1995. Natural graphitization of anthracite: experimental considerations. Carbon 33, 679–691.

Chazhengina, S.Y., Kovalevski, V.V., 2013. Structural characteristics of shungite carbon

subjected to contact metamorphism overprinted by greenschist-facies regional metamorphism. Eur. J. Mineral. 25, 835–843.
Colomban, P., 2002. Analysis of strain and stress in ceramic, polymer and metal matrix composites by Raman spectroscopy. Adv. Eng. Mater. 4, 535–542.
Črne, A., Melezhik, V., Lepland, A., Fallick, A., Prave, A., Brasier, A., 2014. Petrography and geochemistry of carbonate rocks of the Paleoproterozoic Zaonega Formation, Russia: documentation of 13 C-depleted non-primary calcite. Precambrian Res. 240, 79–93.
Črne, A.E., Melezhik, V.A., Prave, A.R., Lepland, A., Romashkin, A.E., Rychanchik, D.V., Hanski, E.J., Luo, Z.Y., 2013a. Zaonega Formation: FAR-DEEP Holes 12A and 12B, and neighbouring quarries. In: Melezhik, V.A., Fallick, A.E., Kump, L.R., Lepland, A., Prave, A.R., Strauss, H. (Eds.), Reading the Archive of Earth's Oxygenation. Springer, pp. 946–1007.
Črne, A.E., Melezhik, V.A., Prave, A.R., Lepland, A., Romashkin, A.E., Rychanchik, D.V., Hanski, E.J., Luo, Z.Y., 2013b. Zaonega Formation: FAR-DEEP Hole 13A. In: Melezhik, V.A., Fallick, A.E., Kump, L.R., Lepland, A., Prave, A.R., Strauss, H. (Eds.), Reading the Archive of Earth's Oxygenation. Springer, pp. 1008–1046.
Delarue, F., Rouzaud, J.-N., Derenne, S., Bourbin, M., Westall, F., Kremer, B., Sugitani, K., Deldicque, D., Robert, F., 2016. The Raman-derived carbonization continuum: A tool to select the best preserved molecular structures in Archean kerogens. Astrobiology 16, 407–417.
Duda, J.-P., Thiel, V., Bauersachs, T., Mißbach, H., Reinhardt, M., Schäfer, N., Van Kranendonk, M.J., Reitner, J., 2018. Ideas and perspectives: hydrothermally driven redistribution and sequestration of early Archaean biomass - the "hydrothermal pump hypothesis". Biogeosciences 15, 1535–1548.
Fallick, A., Melezhik, V., Brasier, A., Prave, A., 2016. Unusual, basin-scale, fluid–rock interaction in the Palaeoproterozoic Onega basin from Fennoscandia: Preservation in calcite δ18O of an ancient high geothermal gradient. Precambrian Res. 281, 224–235.
Ferrari, A.C., Robertson, J., 2000. Interpretation of Raman spectra of disordered and amorphous carbon. Phys. Rev. B 61, 14095–14107.
Filippov, M.M., Golubev, A., 1994. Carbon isotope composition of shungite rocks. The Organic Matter of Karelian Shungite Rocks (Genesis, Evolution and the Methods of Study). Karelian Research Centre, Petrozavodsk, pp. 32–43.
Foucher, F., Ammar, M.-R., Westall, F., 2015. Revealing the biotic origin of silicified Precambrian carbonaceous microstructures using Raman spectroscopic mapping, a potential method for the detection of microfossils on Mars. J. Raman Spectrosc. 46, 873–879.
Galdobina, L.P., 1987. Lyudikovian horizon. In: Sokolov, V.A. (Ed.), The Geology of Karelia. Nauka, Leningrad, pp. 59–67.
Gouadec, G., Colomban, P., 2007. Raman Spectroscopy of nanomaterials: How spectra relate to disorder, particle size and mechanical properties. Prog. Cryst. Growth Character. Mater. 53, 1–56.
Hannah, J.L., Stein, H.J., Zimmerman, A., Yang, G., Melezhik, V.A., Filippov, M.M., Turgeon, S.C., Creaser, R.A., 2008. Re-Os geochronology of shungite: a 2.05 Ga fossil oil field in Karelia. Geochim. Cosmochim. Acta 72, A351.
Henry, D.G., Jarvis, I., Gillmore, G., Stephenson, M., 2019. Raman spectroscopy as a tool to determine the thermal maturity of organic matter: Application to sedimentary, metamorphic and structural geology. Earth-Science Reviews 198. https://doi.org/10.1016/j.earscirev.2019.102936.
Jehlička, J., Bény, C., 1992. Application of Raman microspectrometry in the study of structural changes in Precambrian kerogens during regional metamorphism. Org. Geochem. 18, 211–213.
Khavari-Khorasani, 1979. The nature of Karelian shungite. Chem. Geol. 26, 165–182.
Koistinen, T., Stephens, M.B., Bogatchev, V., Nordgulen, Ø., Wennerström, M., Korhonen, J., 2001. Geological Map of the Fennoscandian Shield, Scale 1:2 000 000. Geological Surveys of Finland, Norway and Sweden and the North-West Department of Natural Resources of Russia.
Kouketsu, Y., Mizukami, T., Mori, H., Endo, S., Aoya, M., Hara, H., Nakamura, D., Wallis, S., 2014. A new approach to develop the Raman carbonaceous material geothermometer for low-grade metamorphism using peak width. Island Arc 23, 33–50.
Kovalevski, V.V., 1994. Structure of shungite carbon. Russ. J. Inorg. Chem. 39, 28–32.
Kovalevski, V.V., Buseck, P.R., Cowley, J.M., 2001. Comparison of carbon in shungite rocks to other natural carbons: an X-ray and TEM study. Carbon 39, 243–256.
Kreitsmann, T., Külaviir, M., Lepland, A., Paiste, K., Paiste, P., Prave, A., Sepp, H., Romashkin, A., Rychanchik, D., Kirsimäe, K., 2019. Hydrothermal dedolomitisation of carbonate rocks of the Paleoproterozoic Zaonega Formation, NW Russia—implications for the preservation of primary C isotope signals. Chem. Geol. 512, 43–57.
Kump, L.R., Junium, C., Arthur, M.A., Brasier, A., Fallick, A., Melezhik, V., Lepland, A., Crne, A.E., Luo, G.M., 2011. Isotopic evidence for massive oxidation of organic matter following the great oxidation event. Science 334, 1694–1696.
Lahfid, A., Beyssac, O., Deville, E., Negro, F., Chopin, C., Goffe, B., 2010. Evolution of the Raman spectrum of carbonaceous material in low-grade metasediments of the Glarus Alps (Switzerland). Terra Nova 22, 354–360.
Martin, A., Prave, A., Condon, D., Lepland, A., Fallick, A., Romashkin, A., Medvedev, P., Rychanchik, D., 2015. Multiple Palaeoproterozoic carbon burial episodes and excursions. Earth Planet. Sci. Lett. 424, 226–236.
Maslova, O., Ammar, M., Guimbretière, G., Rouzaud, J.-N., Simon, P., 2012. Determination of crystallite size in polished graphitized carbon by Raman spectroscopy. Phys. Rev. B 86, 134205.
Melezhik, V., Prave, A.R., Hanski, E.J., Fallick, A.E., Lepland, A., Kump, L.R., Strauss, H., 2012. Reading the Archive of Earth's Oxygenation: Volume 3: Global Events and the Fennoscandian Arctic Russia-Drilling Early Earth Project. Springer Science & Business Media.
Melezhik, V.A., Fallick, A.E., Filippov, M.M., Larsen, O., 1999. Karelian shungite – an indication of 2.0-Ga-old metamorphosed oil-shale and generation of petroleum: geology, lithology and geochemistry. Earth-Sci. Rev. 47, 1–40.
Melezhik, V.A., Filippov, M.M., Romashkin, A.E., 2004. A giant Palaeoproterozoic deposit of shungite in NW Russia: genesis and practical applications. Ore Geol. Rev. 24, 135–154.
Melezhik, V.A., Huhma, H., Condon, D.J., Fallick, A.E., Whitehouse, M.J., 2007. Temporal constraints on the Paleoproterozoic Lomagundi-Jatuli carbon isotopic event. Geology 35, 655–658.
Olcott Marshall, A., Jehlička, J., Rouzaud, J.-N., Marshall, C.P., 2014. Multiple generations of carbonaceous material deposited in Apex chert by basin-scale pervasive hydrothermal fluid flow. Gondwana Res. 25, 284–289.
Ovchinnikova, G.V., Kuznetsov, A.B., Melezhik, V.A., Gorokhov, I.M., Vasil'eva, I.M., Gorokhovskii, B.M., 2007. Pb-Pb age of Jatulian carbonate rocks: the Tulomozero Formation of southeast Karelia. Stratigr. Geol. Correl. 15, 359–372.
Puchtel, I.S., Arndt, N.T., Hofmann, A.W., Haase, K.M., Kröner, A., Kulikov, V.S., Kulikova, V.V., Garbe-Schönberg, C.-D., Nemchin, A.A., 1998. Petrology of mafic lavas within the Onega plateau, central Karelia: evidence for 2.0 Ga plume-related continental crustal growth in the Baltic Shield. Contrib. Mineral. Petrol. 130, 134–153.
Puchtel, I.S., Brugmann, G.E., Hofmann, A.W., 1999. Precise Re-Os mineral isochron and Pb-Nd-Os isotope systematics of a mafic-ultramafic sill in the 2.0 Ga Onega plateau (Baltic Shield). Earth Planet. Sci. Lett. 170, 447–461.
Qu, Y., Črne, A.E., Lepland, A., van Zuilen, M.A., 2012. Methanotrophy in a Paleoproterozoic oil field ecosystem, Zaonega Formation, Karelia, Russia. Geobiology 10, 467–478.
Qu, Y., Engdahl, A., Zhu, S., Vajda, V., McLoughlin, N., 2015. Ultrastructural heterogeneity of carbonaceous material in ancient cherts: investigating biosignature origin and preservation. Astrobiology 15, 825–842.
Qu, Y., Lepland, A., van Zuilen, M.A., Whitehouse, M., Črne, A.E., Fallick, A.E., 2018. Sample-scale carbon isotopic variability and diverse biomass in the Paleoproterozoic Zaonega Formation, Russia. Precambrian Res. 315, 222–231.
Qu, Y., McLoughlin, N., van Zuilen, M.A., Whitehouse, M., Engdahl, A., Vajda, V., 2019. Evidence for molecular structural variations in the cytoarchitectures of a Jurassic plant. Geology 47, 325–329.
Rouzaud, J.-N., Deldicque, D., Charon, E., Pageot, J., 2015. Carbons at the heart of questions on energy and environment: a nanostructural approach. Comptes Rendus Geosci. 347, 124–133.
Sforna, M., van Zuilen, M., Philippot, P., 2014. Structural characterization by Raman hyperspectral mapping of organic carbon in the 3.46 billion-year-old Apex chert, Western Australia. Geochim. Cosmochim. Acta 124, 18–33.
Tuinstra, F., Koenig, J.L., 1970. Raman spectrum of graphite. J. Chem. Phys. 53, 1126.
Ueno, Y., Yamada, K., Yoshida, N., Maruyama, S., Isozaki, Y., 2006. Evidence from fluid inclusions for microbial methanogenesis in the early Archaean era. Nature 440, 516–519.
van den Boorn, S.H., van Bergen, M.J., Nijman, W., Vroon, P.Z., 2007. Dual role of seawater and hydrothermal fluids in Early Archean chert formation: evidence from silicon isotopes. Geology 35, 939–942.
van Zuilen, M., Mathew, K., Wopenka, B., Lepland, A., Marti, K., Arrhenius, G., 2005. Nitrogen and argon isotopic signatures in graphite from the 3.8-Ga-old Isua Supracrustal Belt, Southern West Greenland. Geochim. Cosmochim. Acta 69, 1241–1252.
van Zuilen, M.A., Fliegel, D., Wirth, R., Lepland, A., Qu, Y., Schreiber, A., Romashkin, A.E., Philippot, P., 2012. Mineral-templated growth of natural graphite films. Geochim. Cosmochim. Acta 83, 252–262.
Wopenka, B., Pasteris, J.D., 1993. Structural characteristics of kerogens to granulite-facies graphite: applications of Raman microprobe spectroscopy. Am. Mineral. 78, 533–557.